International Journal of Non–Linear Mechanics 174 (2025) 105083

Contents lists available at ScienceDirect

International Journal of Non-Linear Mechanics

journal homepage: www.elsevier.com/locate/nlm

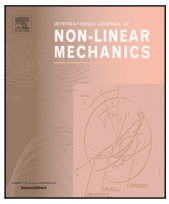

Robust control design of nonlinear negative stiffness base isolators for MDOF systems

Sudip Chowdhury [a],*, Sondipon Adhikari [a], Arnab Banerjee [b]

[a] Glasgow Computational Engineering Centre, James Watt School of Engineering, The University of Glasgow, Glasgow, Scotland, United Kingdom
[b] Civil Engineering Department, Indian Institute of Technology Delhi, India

ARTICLE INFO

Keywords:
Nonlinear negative stiffness base isolators
Multi-degree-of-freedom systems
H_2 optimisation approach
Traditional base isolators

ABSTRACT

Seismic isolation is crucial for protecting structures from earthquake-induced vibrations, yet traditional base isolators (TBI) often exhibit limitations in mitigating dynamic responses, particularly in multi-degree-of-freedom (MDOF) systems. This study introduces nonlinear negative stiffness base isolators (NNBI) as an advanced alternative, leveraging H_2 optimisation to enhance vibration control. A mathematical framework was developed to derive closed-form expressions for optimal NNBI design parameters, followed by numerical validation through frequency and time-domain analyses, including harmonic excitations, random white noise, and near-field earthquake simulations. Results demonstrated that NNBI achieves at least 47.90 % greater dynamic response reduction compared to TBI, with a maximum improvement of 97.80 % for ten DOF systems, confirming its superior energy dissipation capabilities. These findings establish NNBI as a transformative solution for seismic resilience, with potential applications in tall buildings.

1. Introduction

Base isolation, sometimes referred to as seismic isolation or earthquake isolation, is a structural engineering method employed to safeguard buildings and other structures against the detrimental consequences of earthquakes. The main goal of base isolation is to separate the superstructure (the building or structure above ground) from the ground motion caused by an earthquake. This helps to decrease the transfer of seismic forces and prevent excessive lateral movement and shaking [1]. Elastomeric bearings, sliding bearings, laminated rubber bearings, lead rubber bearings, inerter-based isolators, nonlinear damping amplifier friction bearings [2], and inertial amplifier-based isolators are commonly used base isolation systems for controlling the dynamic responses of structures subjected to earthquake excitations [3–8]. These systems are applied to dynamic systems to mitigate the effects of seismic activity [9,10].

In order to acquire a strong ability to reduce dynamic response, the design characteristics of these isolators must be improved. The H_2 optimisation method is a well-known analytical optimisation method. The closed-form formulas in [11] can be used to calculate the best design parameters using this method. This approach is suitable for isolated structures that are energised randomly. One way to improve the effectiveness of isolators in reducing vibrations is to raise their static mass. This causes the base layer to become excessively flexible during seismic occurrences. Furthermore, the base isolator [8] does not effectively function for tall buildings. In order to mitigate these limitations, the isolators are attempting to enhance the effective mass by incorporating inerters and inertial amplifiers, rather than relying solely on static mass. This approach is discussed in the study by Banerjee et al. (2020) [12]. An inerter, sometimes referred to as an inertance device or dynamic vibration absorber, is a mechanical element utilised in engineering and automobile suspension systems. The technology was first offered in the early 2000s as a prospective enhancement to car suspension systems [13]. The primary function of the inerter is to enhance damping by augmenting the effective mass of the isolation systems. An inerter is defined by its property of exerting a force that is directly proportionate to the difference in acceleration between its two ends. Consequently, the inerter produces a force that counteracts the movement between objects, supplying more damping. Islam and Jangid (2024) introduced a novel optimisation approach for negative stiffness and inerter-based dampers [14], demonstrating their effectiveness in enhancing seismic performance by reducing both base displacement and sloshing responses in base-isolated liquid storage tanks [15,16]. Numerous studies are currently dedicated to developing autonomous semi-active control principles and streamlined semi-active control algorithms to mitigate seismic reactions [17]. The purpose of the technique is to generate appropriate hysteretic loops that can efficiently absorb a maximum amount of energy using semi-active devices. The control

* Corresponding author.
E-mail address: Sudip.Chowdhury@glasgow.ac.uk (S. Chowdhury).

https://doi.org/10.1016/j.ijnonlinmec.2025.105083
Received 16 August 2024; Received in revised form 2 March 2025; Accepted 10 March 2025
Available online 18 March 2025

strategy simply necessitates data on the device's displacement and velocity [18]. The semi-active control used in this study produces hysteretic loops that can absorb energy with a capacity similar to friction dampers. However, it mitigates the drawbacks associated with friction dampers, such as residual displacement following strong earthquakes and the generation of high-frequency damping forces [19]. Extensive study has been carried out on the advancement of autonomous negative stiffness dampers to decrease absolute responses [20]. Inertial amplifiers, as described in the study by Adhikari et al. (2022), are devices that effectively amplify mass to strengthen the damping of isolation systems. Furthermore, it can offer increased adaptability while maintaining enough load-bearing capacity in conjunction with the isolators during seismic occurrences. Consequently, the lowermost layer of the isolators may remain intact, thereby potentially extending the lifespan of the isolated structures. Furthermore, passive vibration isolation systems employ various negative stiffness devices, such as quasi-zero stiffness, high-static-low-dynamic stiffness, Euler buckled beams, pseudo-negative-stiffness, negative-stiffness inclusions, and magnetic negative stiffness dampers, to enhance vibration reduction and overcome the constraints of traditional isolators [21]. Therefore, these explicit devices can be seen as an indirect method to enhance the impact of inertia on the additional mass by utilising the force of the negative stiffness element, without really increasing the mass itself. A negative stiffness device is employed to provide rigidity in the opposite direction to that of conventional materials. This concept is extensively employed in the field of structural engineering and vibration control to achieve precise mechanical characteristics or reduce undesirable vibrations. A negative stiffness device operates on the fundamental premise of utilising materials or combinations that demonstrate a negative stiffness characteristic under specific circumstances [22]. These devices frequently undergo deformation in the opposite direction of the applied force, resulting in a reduction in the overall stiffness of the system. Nevertheless, when the force is augmented, the device undergoes a phase shift, resulting in stiffness in the opposite direction and impeding deformation. Negative stiffness devices can be used to reduce vibrations in structures or equipment by providing resistance against the vibrational forces. This is especially beneficial for buildings or intricate equipment where minimising vibration is essential. Negative stiffness devices, like foundation isolation systems, can safeguard buildings and infrastructure against earthquake damage by effectively absorbing seismic energy and minimising the transmission of stresses to the structure. The incorporation of negative stiffness components in mechanical systems can yield specific performance enhancements such as enhanced energy absorption, heightened stability, or greater dynamic responsiveness. However, there are currently no advanced applications available for accurate nonlinear negative stiffness devices designed specifically for isolating vibrations [23]. There are only two alternatives: utilising quasi-zero stiffness and linear negative stiffness devices. These possess limitations and disadvantages that are similar to those of conventional vibration isolation devices. In addition, the effectiveness of a traditional base isolation system in reducing dynamic response can be improved by incorporating a nonlinear negative stiffness device within its core material. This substitution can result in reduced construction and maintenance costs, replacing rotational mass amplification devices, geometrical mass amplification devices, linear negative stiffness devices, and quasi-zero stiffness devices. The nonlinear negative stiffness device can overcome the constraints of ordinary base isolators. Consequently, the proposed technique may outperform current cutting-edge strategies. There is a lack of advanced publications that offer accurate mathematical calculations for the optimal design parameters of the proposed nonlinear vibration isolation device. Isolated structures do not have precise closed-form formulas for perfect nonlinear dynamic reactions. In order to ensure safety and functionality, it is crucial to minimise the dynamic responses of structures that are subjected to external forces such as earthquakes and strong winds. The efficacy of traditional vibration isolation approaches in mitigating nonlinear vibrations is restricted. As a result, a specific area for the study is identified. Furthermore, to enhance the dependability and efficiency of the traditional base isolators, nonlinear negative stiffness devices incorporating helical springs are incorporated into the core materials of the isolators. Currently, there is a lack of analytical closed-form expressions for optimal design parameters for applying precise nonlinear negative stiffness devices to isolators in order to reduce the dynamic responses of multiple degrees of freedom systems [24]. Thus, a deficiency in research is recognised.

This work introduces the nonlinear negative stiffness base isolators (NNBI) to fill the research gap. The concept of the nonlinear negative stiffness base isolator involves the placement of an extra isolator beneath the primary structure. These isolators are used to reduce the dynamic responses of multiple degrees of freedom systems (MDOF). The H_2 optimisation approach is utilised to develop the mathematical expressions for the optimal design parameters for NNBI applied to systems with many degrees of freedom. The frequency response function has been formulated by studying harmonic and random white noise excitations in order to ascertain the frequency domain responses of the isolated structures. Furthermore, the accuracy of the analytical results is confirmed through a numerical investigation. The Newmark-beta method was utilised to conduct a numerical investigation and ascertain the temporal domain replies. Furthermore, a load–displacement hysteresis curve of the NNBI has been determined using numerical modelling in order to comprehend the device's capability. The improved dynamic response reduction capacity (%) of NNBI is obtained by comparing the dynamic responses of NNBI-controlled MDOF systems with traditional base isolators (TBI)-controlled MDOF systems.

2. Structural model and equations of motion

Fig. 1(a) exhibits the structural configuration of a multi-degrees-of-freedom (MDOF) system isolated by nonlinear negative stiffness base isolators. In addition, the schematic diagrams of nonlinear negative stiffness base isolators (NNBI) are shown in Fig. 1(b). An adjacent moat wall is not considered in this study. Therefore, the model of the base-isolated structure (refer to Fig. 1) in the present study considers the flexibility of the superstructures but ignores the impact at the base with the adjacent moat wall [25,26]. $\ddot{z}_g$ defines the base excitation. The top degree of freedom (DOF)'s mass, stiffness, and damping ratio are defined as m_j, k_j, and c_j. The second DOF's mass, damping, and stiffness are defined as m_{j-1}, c_{j-1}, and k_{j-1}; m_1, c_1, and k_1 define the mass, damping, and stiffness of the first degree of freedom system. The governing equations of motion of the multi degrees of freedom (MDOF) system isolated by NNBI are derived using Lagrange's equation and expressed as

$$m_b\ddot{z}_b + c_b\dot{z}_b + k_b z_b + k_r z_b\left(1 - \frac{L_o}{\sqrt{z_b^2 + L^2}}\right) - c_1\dot{z}_1 - k_1 z_1 = -m_b\ddot{z}_g$$
$$[M]\{\ddot{z}\} + [C]\{\dot{z}\} + [K]\{z\} = -[M]\{r\}(\ddot{z}_g + \ddot{z}_b) \tag{1}$$

where L_o and L define the free and forced length of the nonlinear helical spring. $\{r\}$ defines the vector with unity for all its elements [27]. In order to generalise the nonlinear governing equation of motion and to achieve the optimal parameters for the NNBI utilising the H_2 optimisation approach, the Taylor series expansion is used for the Eq. (1). z_b defines the relative displacement of the isolator with respect to ground. z defines the relative displacement vector of each floor of the superstructure with respect to the isolator. Consequently, these are the generalised nonlinear governing equations of motion:

$$m_b\ddot{z}_b + c_b\dot{z}_b + k_b z_b - k_r\left(\frac{L_o}{L}\right)z_b - k_r z_b + \left(\frac{L_o}{2L^3}\right)k_r z_b^3 - c_1\dot{z}_1 - k_1 z_1 = -m_b\ddot{z}_g$$
$$[M]\{\ddot{z}\} + [C]\{\dot{z}\} + [K]\{z\} = -[M]\{r\}(\ddot{z}_g + \ddot{z}_b) \tag{2}$$

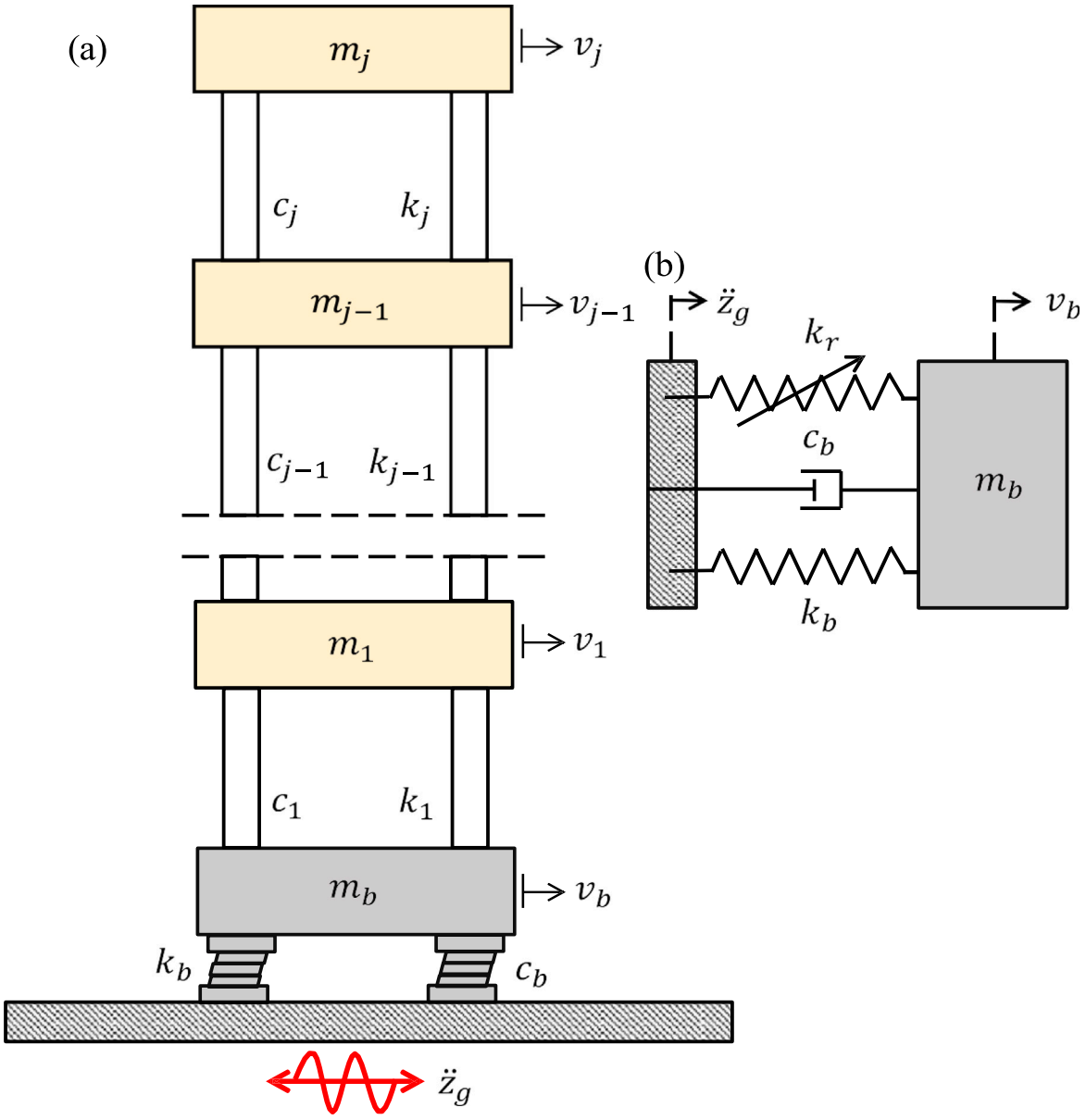

Fig. 1. (a) A multi-degrees-of-freedom system is isolated by nonlinear negative stiffness base isolators (NNBI) under base excitation. (b) The schematic diagram of NNBI.

Each nonlinear component of Eq. (2) is linearised using the statistical linearisation technique [28]. The linearised governing equations of motion of the isolated structure are derived as

$$\begin{aligned} &m_b\ddot{z}_b + c_b\dot{z}_b + k_b z_b - k_r\left(\frac{L_o}{L}+1\right)z_b + 3\sigma_{z_b}^2\left(\frac{L_o}{2L^3}\right)k_r z_b \\ &\quad - c_1\dot{z}_1 - k_1 z_1 = -m_b\ddot{z}_g \\ &[M]\{\ddot{z}\} + [C]\{\dot{z}\} + [K]\{z\} = -[M]\{r\}(\ddot{z}_g + \ddot{z}_b) \end{aligned} \tag{3}$$

An error may be occurred during the transformation of the linearised term from the nonlinear stiffness element in Eq. (2) using the statistical linearisation technique. The error has been derived as

$$\begin{aligned} W_r &= \left(\frac{L_o}{2L^3}\right)k_r z_b^3 - \underbrace{3\sigma_{z_b}^2\left(\frac{L_o}{2L^3}\right)k_r z_b}_{\Phi_r} \\ \frac{\partial W_r^2}{\partial \Phi_r} &= E\left\{\left(\left(\frac{L_o}{2L^3}\right)k_r z_b^3 - \Phi_r z_b\right)^2\right\} = 0 \end{aligned} \tag{4}$$

No error occurs during the statistical linearisation process. Accordingly, $\sigma_{z_b}^2$ is applicable [29]. Initially, $\sigma_{z_b}^2 = 0$ considers to carry out H_2 optimisation techniques. As a result, the changed equations of motion are as follows:

$$\begin{aligned} &m_b\ddot{z}_b + c_b\dot{z}_b + k_b z_b - \kappa k_r z_b - c_1\dot{z}_1 - k_1 z_1 = -m_b\ddot{z}_g \\ &[M]\{\ddot{z}\} + [C]\{\dot{z}\} + [K]\{z\} = -[M]\{r\}(\ddot{z}_g + \ddot{z}_b) \end{aligned} \tag{5}$$

where $\kappa = \left(\frac{L_o}{L}+1\right)$ and $\alpha = k_r/k_b$. α defines the negative stiffness ratio. The superstructure's displacement vector is determined as $z = \{z_1, z_2, z_3, z_4, z_5, \ldots, z_j\}^T$. The steady-state solutions for harmonic base excitation are considered as $z = Ze^{i\omega t}$, $z_b = Z_b e^{i\omega t}$, and $\ddot{z}_g = Z_g e^{i\omega t}$. The transfer function is calculated as follows:

$$\begin{bmatrix} H_1 & H_2 & 0 & 0 & 0 & q^2 \\ H_2 & H_1 & H_2 & 0 & 0 & q^2 \\ 0 & H_2 & H_1 & H_2 & 0 & q^2 \\ 0 & 0 & H_2 & H_1 & H_2 & q^2 \\ 0 & 0 & 0 & H_2 & H_3 & q^2 \\ H_2 & 0 & 0 & 0 & 0 & H_4 \end{bmatrix} \begin{Bmatrix} Z_1 \\ Z_2 \\ Z_3 \\ Z_4 \\ Z_5 \\ Z_b \end{Bmatrix} = -\begin{bmatrix} 1 \\ 1 \\ 1 \\ 1 \\ 1 \\ \mu_b \end{bmatrix} Z_g \tag{6}$$

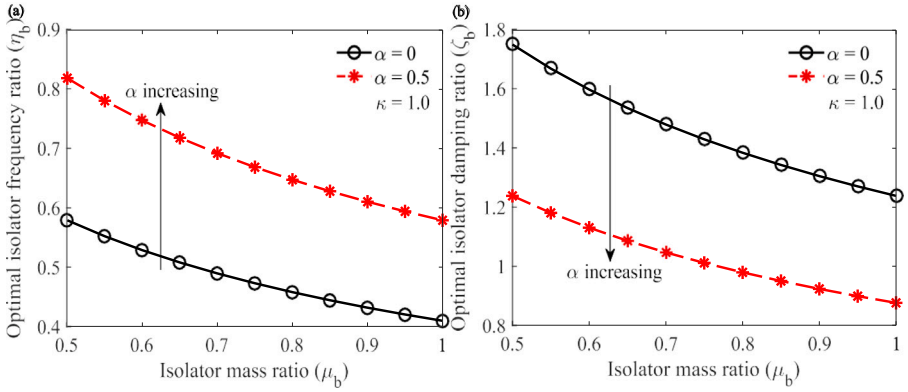

Fig. 2. The variations of the optimal (a) frequency and (b) damping ratios of NNBI for negative stiffness ratios $\alpha = 0$ and $\alpha = 0.5$.

where

$$q = \mathrm{i}\omega,\ H_1 = 4\,\zeta_s q\omega_s + q^2 + 2\,{\omega_s}^2,\ H_2 = -2\,\zeta_s q\omega_s - {\omega_s}^2,$$
$$H_3 = 2\,\zeta_s q\omega_s + q^2 + {\omega_s}^2, \quad \text{and} \quad H_4 = -\kappa\,\alpha\,\mu_b\,{\omega_b}^2 + 2\,\mu_b\,\zeta_b\,\omega_b\,q + \mu_b\,{\omega_b}^2 + \mu_b q^2 \tag{7}$$

Considers $\zeta_s = 0$, and the dynamic response of the top DOF is determined as

$$G_5 = \left.\frac{Z_5}{Z_g}\right|_{q=\mathrm{i}\omega} = \frac{\begin{pmatrix} -\left(q^4 + 5\,q^2{\omega_s}^2 + 5\,{\omega_s}^4\right)\mu_b\,\omega_b\,\left(q^2 + {\omega_s}^2\right) \\ \left(\alpha\,\kappa\,\omega_b - 2\,q\zeta_b - \omega_b\right)\left(q^2 + 3\,{\omega_s}^2\right) \end{pmatrix}}{\Delta_g} \tag{8}$$

The dynamic response of the NNBI is determined as

$$G_b = \left.\frac{Z_b}{Z_g}\right|_{q=\mathrm{i}\omega} = \frac{\begin{pmatrix} q^{10}\mu_b + 9\,q^8\mu_b{\omega_s}^2 + 28\,q^6\mu_b{\omega_s}^4 + 35\,q^4\mu_b{\omega_s}^6 \\ +15\,q^2\mu_b{\omega_s}^8 + \mu_b{\omega_s}^{10} + q^8{\omega_s}^2 + 8\,q^6{\omega_s}^4 \\ +21\,q^4{\omega_s}^6 + 20\,q^2{\omega_s}^8 + 5\,{\omega_s}^{10} \end{pmatrix}}{\Delta_g} \tag{9}$$

The denominator Δ_g is derived as

$$\begin{aligned} \Delta_g = {} & q^{12}\mu_b + 2\,\mu_b\,q^{11}\zeta_b\,\omega_b + \left(-{\omega_b}^2\kappa\,\alpha\,\mu_b + {\omega_b}^2\mu_b + 9\,\mu_b{\omega_s}^2 + {\omega_s}^2\right)q^{10} \\ & +18\,\mu_b\,q^9\zeta_b\,\omega_b\,{\omega_s}^2 + \left(-9\,\alpha\,\kappa\,\mu_b\,{\omega_b}^2{\omega_s}^2 + 9\,\mu_b\,{\omega_b}^2{\omega_s}^2 + 28\,\mu_b{\omega_s}^4 + 8\,{\omega_s}^4\right)q^8 \\ & +56\,\mu_b\,q^7\zeta_b\,\omega_b\,{\omega_s}^4 + \left(-28\,\alpha\,\kappa\,\mu_b\,{\omega_b}^2{\omega_s}^4 + 28\,\mu_b\,{\omega_b}^2{\omega_s}^4 + 35\,\mu_b{\omega_s}^6 + 21\,{\omega_s}^6\right)q^6 \\ & +70\,\mu_b\,q^5\zeta_b\,\omega_b\,{\omega_s}^6 + \left(-35\,\alpha\,\kappa\,\mu_b\,{\omega_b}^2{\omega_s}^6 + 35\,\mu_b\,{\omega_b}^2{\omega_s}^6 + 15\,\mu_b{\omega_s}^8 + 20\,{\omega_s}^8\right)q^4 \\ & +30\,\mu_b\,q^3\zeta_b\,\omega_b\,{\omega_s}^8 + \left(-15\,\alpha\,\kappa\,\mu_b\,{\omega_b}^2{\omega_s}^8 + 15\,\mu_b\,{\omega_b}^2{\omega_s}^8 + \mu_b{\omega_s}^{10} + 5\,{\omega_s}^{10}\right)q^2 \\ & +2\,\mu_b\,q\zeta_b\,\omega_b\,{\omega_s}^{10} - \alpha\,\kappa\,\mu_b\,{\omega_b}^2{\omega_s}^{10} + \mu_b\,{\omega_b}^2{\omega_s}^{10} \end{aligned} \tag{10}$$

The derived equations highlight the influence of nonlinear negative stiffness on the dynamic response of base-isolated structures, demonstrating its role in modifying system stiffness and damping characteristics. By incorporating the negative stiffness component, the effective stiffness of the isolator is reduced, enabling improved energy dissipation and enhanced vibration mitigation. The next section presents the H_2 optimisation framework, which determines the optimal design parameters for the nonlinear negative stiffness base isolator, ensuring a balance between structural stability and seismic performance.

3. H_2 optimisation

H_2 optimisation implements to derive the optimal closed-form solutions for design parameters, such as natural frequency and damping ratio of novel isolators installed in multi-degrees-of-freedom systems. Random-white noise excitation is applied to perform the optimisation method. Eqs. (8) and (10) applies to derive the standard deviation of the dynamic response of top DOF of the MDOF system [28] and expressed as

$$\sigma^2_{G_5} = \frac{671\,S_0\pi\,\omega_b}{2\,{\omega_s}^6\zeta_b}\left(\left(\frac{20\,\mu_b\,{\zeta_b}^2}{61} - \frac{225\,\alpha\,\kappa}{671} + \frac{225}{671}\right){\omega_s}^2 + \mu_b\,{\omega_b}^2\,(\alpha\,\kappa - 1)^2\right) \tag{11}$$

Eq. (11) differentiates by damping ratio and natural frequency of NNBI, and the mathematical formulations are expressed as

$$\frac{\partial\sigma^2_{G_5}}{\partial\zeta_b} = 0 \quad \text{and} \quad \frac{\partial\sigma^2_{G_5}}{\partial\omega_b} = 0 \tag{12}$$

Eq. (11) is placed in the first equation of Eq. (12) and the closed-form expression for damping ratio NNBI obtains

$$\zeta_b = \frac{\sqrt{55}\sqrt{\mu_b\left(\begin{matrix} 671\,\alpha^2\kappa^2\mu_b\,{\omega_b}^2 - 1342\,\alpha\,\kappa\,\mu_b\,{\omega_b}^2 - 225\,{\omega_s}^2\alpha\,\kappa \\ +671\,\mu_b\,{\omega_b}^2 + 225\,{\omega_s}^2 \end{matrix}\right)}}{110\,\mu_b\,\omega_s} \tag{13}$$

Eq. (13) is placed in Eq. (11), and a modified SD is derived, which contains only the natural frequency of NNBI. Hence, expressed as

$$\sigma^2_{G_5} = \frac{2\,\mu_b\,\sqrt{671}\sqrt{55}\omega_b\,S_0\left(671\,\alpha\,\kappa\,\mu_b\,{\omega_b}^2 - 671\,{\omega_b}^2\mu_b - 225\,{\omega_s}^2\right)\pi\,(\kappa\,\alpha - 1)}{671\sqrt{\left({\omega_b}^2\,(\kappa\,\alpha - 1)\,\mu_b - \frac{225\,{\omega_s}^2}{671}\right)(\kappa\,\alpha - 1)\,\mu_b{\omega_s}^5}} \tag{14}$$

Eq. (14) is placed in the second equation of Eq. (12) and the optimal frequency of NNBI obtains

$$(\omega_b)_{\mathrm{opt}} = \frac{15\omega_s}{\sqrt{1342\,\mu_b - 1342\,\alpha\,\kappa\,\mu_b}} \tag{15}$$

Eq. (15) is placed in Eq. (13) to determine optimal damping ratio for NNBI and obtains

$$(\zeta_b)_{\mathrm{opt}} = \frac{3\sqrt{(1-\alpha\,\kappa)\,\mu_b}\sqrt{330}}{44\,\mu_b} \tag{16}$$

Fig. 2 illustrates the variations in the optimal isolator frequency ratio (η_b) and damping ratio (ζ_b) for different negative stiffness ratios (i.e., $\alpha = 0$ and $\alpha = 0.5$). $\alpha = 0$ corresponds to the case without a negative stiffness device. In Fig. 2(a), the frequency ratio decreases as the isolator mass ratio (μ_b) increases, indicating that heavier isolators tend to have lower optimal frequencies. However, for a given μ_b, increasing the negative stiffness ratio (α) further increases η_b, demonstrating a stiffening effect that raises the system's resonance frequency. This suggests that NNBI with higher negative stiffness operates at higher frequencies, potentially altering its isolation performance.

Fig. 2(b) shows that the optimal damping ratio (ζ_b) decreases as the isolator mass ratio (μ_b) increases, indicating that heavier isolators require less damping for optimal performance. Furthermore, increasing

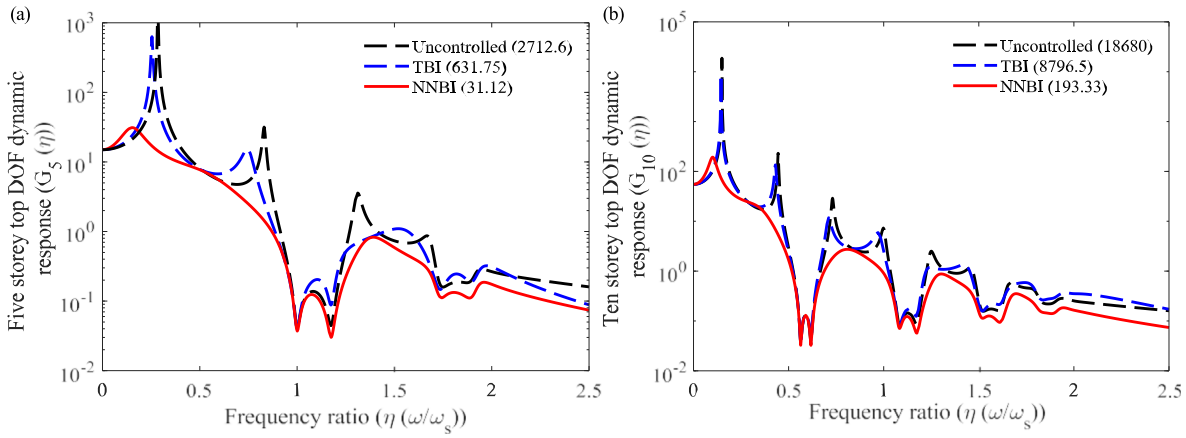

Fig. 3. The optimal dynamic response of uncontrolled, isolated (a) five and (b) ten degrees of freedom systems.

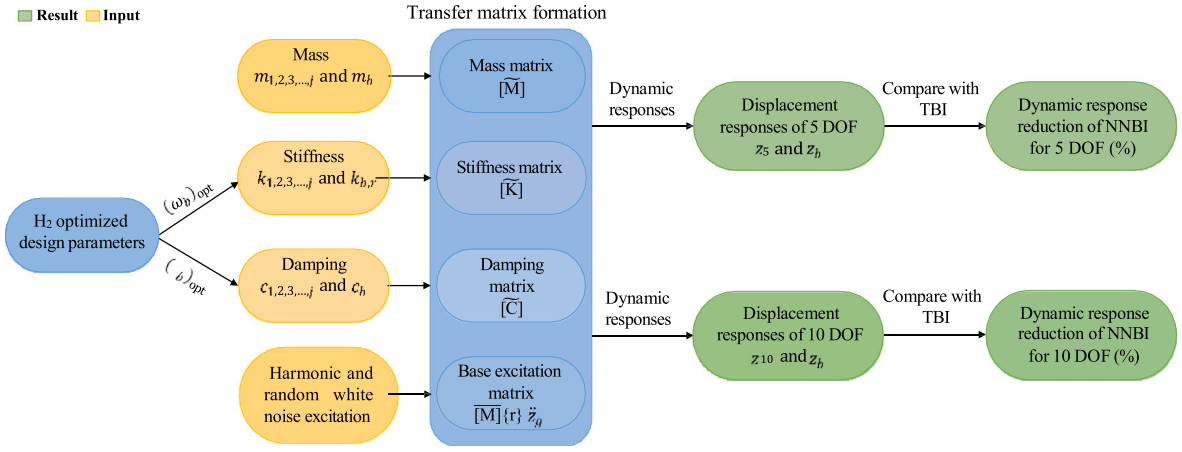

Fig. 4. The algorithm for evaluating the dynamic reduction capacity (%) of NNBI w.r.t TBI.

the negative stiffness ratio (α) leads to a further reduction in ζ_b, suggesting that NNBI systems with a higher negative stiffness ratio achieve effective vibration isolation with lower damping requirements. Notably, ζ_b exceeds unity in certain cases, raising the question of whether the system is over-damped. While a damping ratio greater than unity typically indicates overdamping in classical vibration systems, it does not necessarily imply the same for tuned vibration isolators. In the present study, the optimal damping ratio (ζ_b) is determined based on performance criteria that balance vibration isolation and energy dissipation. A damping ratio exceeding unity does not imply an over-damped system but rather an optimised design where the damping is tuned to enhance isolation efficiency. This is particularly relevant for nonlinear negative stiffness base isolators, where the interplay between stiffness nonlinearity and damping leads to improved performance without significantly compromising system responsiveness. These findings highlight the potential of NNBI in achieving efficient vibration control by strategically leveraging negative stiffness to fine-tune frequency and damping characteristics.

4. Dynamic response evaluation

The optimal design parameters for NNBI and traditional base isolators (TBI) [26] are listed in Table 1. The mass ratio for both isolators is taken at 1.1. The damping ratio of each degree of freedom is taken at 0.01. The system parameter for each degree of freedom is listed in Table 2.

Table 1
H_2 optimised system parameters for isolators.

System	Proposed by	H_2 optimisation	
		η_b	ζ_b
NNBI	This study	0.5521	0.8351
TBI	Matsagar and Jangid [26]	0.5	0.1

Conventional BI: base mass ratio (μ_B) = 1, NNBI: isolator mass ratio (μ_b) = 1, Mass ratio: $\mu_b = \mu_B$. $\kappa = 1.0$ and $\alpha = 0.5$.

Table 2
System parameters of main structures (uncontrolled and controlled structures).

Name	Symbol	Values
Damping ratio	ζ_s	0.01

4.1. Frequency domain analysis

For this study, five and ten degrees of freedom are taken. The optimal dynamic response of uncontrolled, isolated five degrees of freedom systems is shown in Fig. 3(a). The maximum dynamic response of uncontrolled five DOF is obtained 2712.6. In addition, the dynamic responses of five DOF isolated by TBI and NNBI are evaluated 631.75 and 31.12. The dynamic response of NNBI-controlled five DOF is compared with the TBI-controlled five DOF. Accordingly, the dynamic response reduction capacity of NNBI is 95.07% superior to TBI for five DOF. Fig. 3(b) illustrates the optimal dynamic response of an uncontrolled, isolated ten degrees of freedom system. Ten uncontrolled DOF's

Table 3
H_2 optimised system parameters for isolators.

System	Proposed by	H_2 optimisation	
		η_b	ζ_b
NNBI	This study	0.5521	0.8351
TBI	Chowdhury et al. [31]	0.39	0.64

Conventional BI: base mass ratio (μ_B) = 1.1, NNBI: isolator mass ratio (μ_b) = 1.1, Mass ratio: $\mu_b = \mu_B$. $\kappa = 1.0$ and $\alpha = 0.5$.

maximum dynamic response obtains 18 680. The maximum dynamic responses of ten DOF isolated by TBI and NNBI are obtained 8796.5 and 193.33. Accordingly, the dynamic response reduction capacity of NNBI is 97.80% superior to TBI for ten DOF. To evaluate the dynamic response reduction capacity (%) of NNBI for five and ten degrees of freedom systems w.r.t TBI, an analytical algorithm is developed. The algorithm is shown in Fig. 4. The mathematical formulation to derive the dynamic response reduction capacity of NNBI for five and ten degrees of freedom system is derived and expressed as

$$R(\%) = \left(\frac{G_{TBI} - G_{NNBI}}{G_{TBI}}\right) \times 100 \tag{17}$$

G_{TBI} and G_{NNBI} define the maximum dynamic responses of the structures isolated by the traditional base isolator and nonlinear negative stiffness base isolator. The extra experiments are intended to verify the viability of the proposed methodology over a broader variety of seismic excitation scenarios. To do this, the ground acceleration for this study might be the Clough–Penzien power spectrum, a modified version of the well-known Kanai–Tajimi spectrum. The process is unique in that it employs a single-sided PSD.

$$\begin{aligned} Z_{\ddot{z}_g} &= S_0 \frac{\lambda_x^4 + 4\xi_f^2\lambda_x^2\omega^2}{\left(\lambda_x^2 - \omega^2\right)^2 + 4\xi_f^2\lambda_x^2\omega^2} \frac{\omega^4}{\left(\lambda_y^2 - \omega^2\right)^2 + 4\xi_g^2\lambda_y^2\omega^2} \\ &= S_0 \frac{\lambda_x^4 - 4\xi_f^2\lambda_x^2 q^2}{\left(\lambda_x^2 + q^2\right)^2 - 4\xi_f^2\lambda_x^2 q^2} \frac{q^4}{\left(\lambda_y^2 + q^2\right)^2 - 4\xi_g^2\lambda_y^2 q^2} \end{aligned} \tag{18}$$

where S_0 and $q = \mathrm{i}\omega$ denote the constant power spectral density for random white noise excitation. The Kanai–Tajimi model's filter parameters are ξ_f for the soil layer's damping capacity and λ_x for its natural frequency. A second filter with the parameters λ_y and ξ_g provides a limited power output for ground displacement. Because the second quotient $\lambda_y \ll \lambda_x$ quickly approaches unity, the second filter only impacts very low-range frequencies. The filter parameter values for studying areas with firm, medium, and soft soils are extracted from [30]. This analysis takes into account the soft soil condition. The optimal dynamic responses of uncontrolled and isolated structures subjected to random white noise excitation have been shown in Fig. 5. The structural system parameters are listed in Table 3. The maximum dynamic response of uncontrolled five DOF is obtained 9.966×10^8 dB/Hz. In addition, the dynamic responses of five DOF isolated by TBI and NNBI are evaluated 6.496×10^8 dB/Hz and 7.766×10^7 dB/Hz. The dynamic response of NNBI-controlled five DOF is compared with the TBI-controlled five DOF. Accordingly, the dynamic response reduction capacity of NNBI is 88.04% superior to TBI for five DOF.

4.2. Time history analysis

Additionally, a numerical research is employed to support the recommended methodologies. The Newmark-beta method is used to calculate the time history results. The computational environment is used to recreate earthquake-generated reactions in controlled buildings by using pulses to simulate a real earthquake in close proximity to field recordings. The main structure's mass (m_s = 3000 tons) is noted. The structure's time interval is denoted as $T_s = 0.5$ s or 0.5 s. The structure's natural frequency is calculated using its time period, $\omega_s = 2\pi/T_s$.

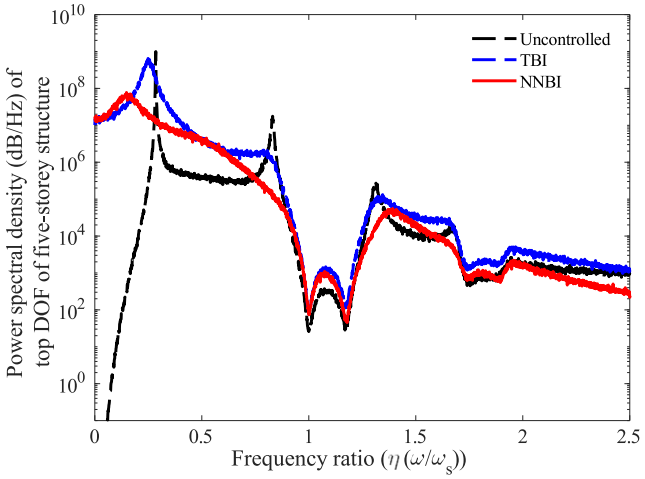

Fig. 5. The optimal dynamic responses of uncontrolled and isolated structures subjected to random white noise excitation.

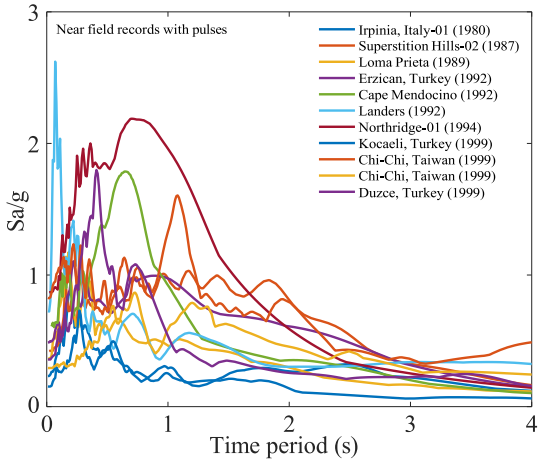

Fig. 6. The spectra of response seen in near field earthquake recordings with pulses, using a damping factor of 5%.

The fundamental structure's viscous damping ratio is assumed to be 0.01; this is represented as $\zeta_s = 0.01$. Table 4 provides a complete list of parameters relevant to near-field earthquake recordings with pulses. Fig. 6 displays the reaction spectra of the near field earthquake records with pulses, accounting for a 5% damping factor. Fig. 7 illustrates the time–history displacement responses of the top degree of freedom (DOF) of a five-storey structure subjected to four different earthquake excitations: Irpinia, Italy-01, Superstition Hills-02, Loma Prieta, and Erzican, Turkey. The comparison between the uncontrolled structure, the traditional base isolator (TBI), and the nonlinear negative stiffness base isolator (NNBI) reveals that NNBI significantly reduces peak displacements in all cases. The uncontrolled structure exhibits the highest displacement, while TBI reduces it moderately. In contrast, NNBI consistently achieves the lowest displacement values, demonstrating superior vibration mitigation. The results indicate that the vibration reduction capacity of NNBI is up to 42% compared to the TBI. The effectiveness of NNBI across different seismic events highlights its robustness in energy dissipation and structural stability. The findings confirm that NNBI is a highly efficient solution for improving seismic resilience in multi-degree-of-freedom structures. The average maximum displacement amplitudes of structures isolated by conventional and novel isolators are compared using Table 5 and substituted into Eq. (19)

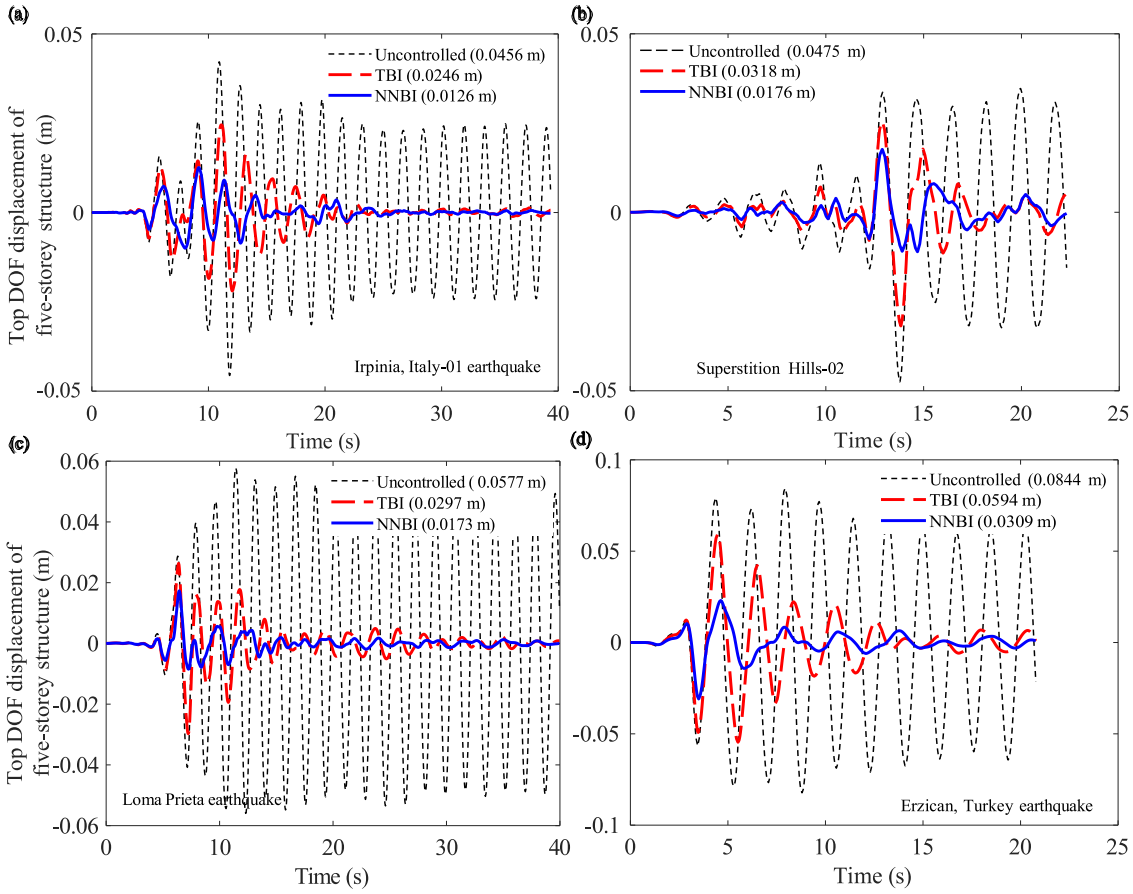

Fig. 7. The variations of displacements of top DOF of five-storey uncontrolled and isolated structures versus time subjected to Irpinia, Italy-01, Superstition Hills-02, Loma Prieta, and Erzican, Turkey earthquakes.

Table 4
The near-field earthquake records.

Earthquake	Year	M_w	Recording station	Vs_{30} (m/s)	Component	E_s (km)	PGA,g
Irpinia, Italy-01	1980	6.9	Sturno	1000	MUL009	30.4	0.31
Superstition Hills-02	1987	6.5	Parachute Test Site	349	SUPERST	16.0	0.42
Loma Prieta	1989	6.9	LOMAP	371	HEC000	27.2	0.38
Erzican, Turkey	1992	6.7	Erzincan 11	275	ERZIKAN	9.0	0.49
Cape Mendocino	1992	7.0	CAPEMEND	713	NIS090	4.5	0.63
Landers	1992	7.3	Lucerne	685	LANDERS	44.0	0.79
Northridge-01	1994	6.7	Rinaldi Receiving Sta	282	NORTHR	10.9	0.87
Kocaeli, Turkey	1999	7.5	Izmit	811	KOCAELI	5.3	0.22
Chi-Chi, Taiwan	1999	7.6	TCU065	306	CHICHI	26.7	0.82
Chi-Chi, Taiwan	1999	7.6	TCU102	714	CHICHI	45.6	0.29
Duzce, Turkey	1999	7.1	Duzce	276	DUZCE	1.6	0.52

to determine the vibration reduction capacity of the novel isolator.

$$D_{G_5}(\%) = \left(\frac{\left(G_5^{max}\right)^{TBI} - \left(G_5^{max}\right)^{NNBI}}{\left(G_5^{max}\right)^{TBI}} \right) \times 100 \tag{19}$$

$D_{G_5}(\%)$ defines the dynamic response reduction capacity of NNBI with respect to TBI. $\left(G_5^{max}\right)^{TBI}$ and $\left(G_5^{max}\right)^{NNBI}$ define the maximum dynamic responses of the top DOF of five storey structures isolated by TBI and NNBI. Table 5 presents a comparative analysis of the maximum displacement responses of uncontrolled, TBI, and NNBI-isolated structures subjected to various near-field earthquake recordings with pulses. The results demonstrate that NNBI consistently achieves the lowest displacement values, outperforming both uncontrolled structures and those equipped with traditional base isolators (TBI). On average, the maximum displacement for NNBI (0.0203 m) is nearly half that of TBI (0.0389 m), highlighting its superior vibration mitigation capabilities. The displacement reduction capacity of NNBI compared to TBI varies across different earthquakes, ranging from 36.1512% to 57.6731%, with the highest reduction observed for the second Chi-Chi, Taiwan earthquake. The findings confirm NNBI's effectiveness in reducing seismic vibrations through its nonlinear negative stiffness mechanism, which enhances energy dissipation while maintaining stability. With an average reduction capacity of 47.92%, NNBI proves to be a highly efficient and reliable solution for improving seismic resilience in multi-degree-of-freedom structures.

Fig. 8 illustrates the hysteresis behaviour of a five-storey structure subjected to different earthquake excitations, comparing the performance of uncontrolled structures, traditional base isolators (TBI), and nonlinear negative stiffness base isolators (NNBI). The uncontrolled structures exhibit the largest hysteresis loops, indicating significant

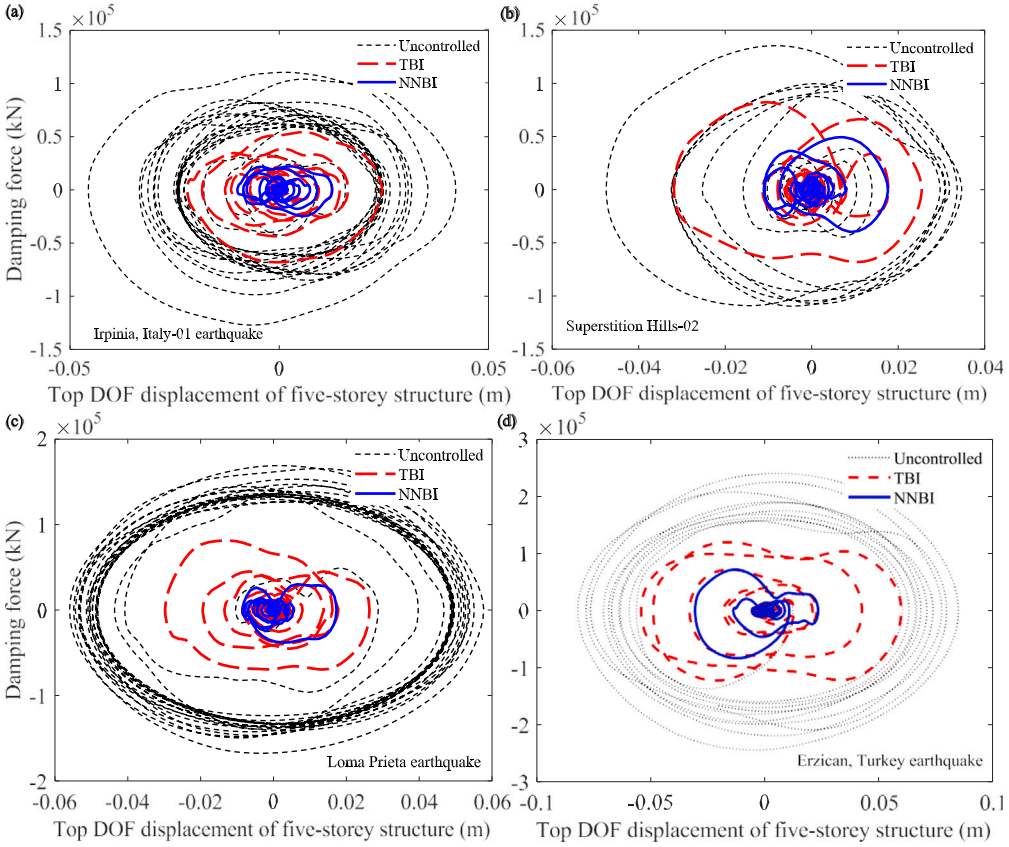

Fig. 8. The variations of displacements of top DOF of five-storey uncontrolled and isolated structures versus time subjected to Irpinia, Italy-01, Superstition Hills-02, Loma Prieta, and Erzican, Turkey earthquakes.

Table 5
The study evaluates the maximum displacement responses of both uncontrolled and isolated structures, assessing the vibration reduction capability of H_2 under near-field earthquake recordings with pulses. The analysis specifically focuses on the optimal NNBI in comparison to TBI.

Earthquake	G_5^{max} (m)			D_{G_5}(%)
	Uncontrolled	TBI	NNBI	NNBI
Irpinia, Italy-01	0.0456	0.0246	0.0126	48.6634
Superstition Hills-02	0.0475	0.0318	0.0176	44.6471
Loma Prieta	0.0577	0.0297	0.0173	41.872
Erzican, Turkey	0.0844	0.0594	0.0309	47.954
Cape Mendocino	0.0512	0.0378	0.0241	36.1512
Landers	0.0238	0.0154	0.007	54.3891
Northridge-01	0.0947	0.072	0.04	44.4647
Kocaeli, Turkey	0.0323	0.0133	0.006	55.1232
Chi-Chi, Taiwan	0.1101	0.0657	0.0278	57.6731
Chi-Chi, Taiwan	0.0605	0.0428	0.0222	48.1197
Duzce, Turkey	0.0525	0.0359	0.0186	48.0635
Average	0.060027273	0.038945455	0.020372727	47.92

displacement and damping force, which suggests substantial energy dissipation through structural deformation, potentially leading to severe damage during seismic events. The TBI-controlled structures demonstrate reduced displacement and force transmission, with moderate energy dissipation, showing improvement over the uncontrolled case but still allowing considerable motion. In contrast, the NNBI-controlled structures exhibit the smallest and most compact hysteresis loops, confirming their superior vibration mitigation capability. NNBI effectively minimises both displacement and damping force, enhancing seismic resilience while maintaining stability. The presence of multiple smaller loops suggests a more adaptive and efficient energy dissipation mechanism. Across different seismic events, NNBI consistently outperforms TBI, highlighting its potential as a more effective solution for protecting multi-degree-of-freedom structures against earthquakes.

5. Summary and conclusions

This paper introduced nonlinear negative stiffness base isolators (NNBI) as an advanced seismic mitigation solution for multi-degree-of-freedom (MDOF) systems, leveraging H_2 optimisation to derive closed-form expressions for optimal design parameters. NNBI achieved at least 47.92% greater dynamic response reduction compared to traditional base isolators (TBI), with its superior performance validated through frequency and time-domain analyses, including harmonic excitations, random white noise, and near-field earthquake simulations. The compact hysteresis loops of NNBI confirmed its enhanced energy dissipation and vibration mitigation capabilities. Key novel contributions include the first-time application of H_2 optimisation to NNBI, a mathematically optimised design framework, and the demonstration of significant seismic resilience improvements. These findings highlight NNBI's potential for multi-storey buildings reducing construction and maintenance costs while ensuring enhanced safety and durability. Future work will focus on experimental validation and AI-based adaptive control, paving the way for next-generation seismic protection technologies.

CRediT authorship contribution statement

Sudip Chowdhury: Writing – review & editing, Writing – original draft, Visualization, Validation, Software, Resources, Project administration, Methodology, Investigation, Funding acquisition, Formal analysis, Data curation, Conceptualization. **Sondipon Adhikari:** Writing

– review & editing, Visualization, Supervision, Project administration, Methodology, Conceptualization. **Arnab Banerjee:** Writing – review & editing, Supervision, Project administration, Conceptualization.

Declaration of competing interest

The authors declare that they have no known competing financial interests or personal relationships that could have appeared to influence the work reported in this paper.

Acknowledgements

The authors would like to acknowledge the Inspire faculty grant, grant number DST/INSPIRE/04/2018/000052 for partial financial support for the project. SC would like to acknowledge the MHRD, India grant received from IIT Delhi during the period of this research work. SC would like to acknowledge the Post Doctoral grant received from The University of Glasgow during the period of this research work.

Data availability

No data was used for the research described in the article.

References

[1] C. Masnata, A. Di Matteo, C. Adam, A. Pirrotta, Smart structures through nontraditional design of tuned mass damper inerter for higher control of base isolated systems, Mech. Res. Commun. 105 (2020) 103513.
[2] S. Chowdhury, S. Adhikari, Nonlinear damping amplifier friction bearings, J. Vib. Acoust. 147 (3) (2025).
[3] G. Quaranta, G. Angelucci, F. Mollaioli, Near-fault earthquakes with pulse-like horizontal and vertical seismic ground motion components: Analysis and effects on elastomeric bearings, Soil Dyn. Earthq. Eng. 160 (2022) 107361.
[4] G. Shi, X. Yu, H. Meng, F. Zhao, J. Wang, J. Jiao, H. Jiang, Effect of surface modification on friction characteristics of sliding bearings: A review, Tribol. Int. (2022) 107937.
[5] J. Sun, G. Zhufu, Mechanical behavior of laminated rubber isolation bearing with buckling steel plate, Int. J. Steel Struct. 22 (4) (2022) 1069–1085.
[6] X. Chen, K. Ikago, Z. Guan, J. Li, X. Wang, Lead-rubber-bearing with negative stiffness springs (LRB-NS) for base-isolation seismic design of resilient bridges: A theoretical feasibility study, Eng. Struct. 266 (2022) 114601.
[7] S. Chowdhury, A. Banerjee, S. Adhikari, The optimal configuration of negative stiffness inerter-based base isolators in multi-storey buildings, in: Structures, Vol. 50, Elsevier, 2023, pp. 1232–1251.
[8] S. Chowdhury, A. Banerjee, S. Adhikari, The optimum inertial amplifier viscoelastic base isolators for dynamic response mitigation of structures: an analytical study, J. Struct. Integr. Maint. (2023) 1–11.
[9] T.-T. Tran, T.-H. Nguyen, D. Kim, Seismic incidence on base-isolated nuclear power plants considering uni-and bi-directional ground motions, J. Struct. Integr. Maint. 3 (2) (2018) 86–94.
[10] D.C. Nguyen, Vibration control of an articulated tower with a tuned mass damper subjected to the inertial force of ground acceleration, J. Struct. Integr. Maint. 7 (3) (2022) 188–197.
[11] S. Chowdhury, A. Banerjee, The exact closed-form expressions for optimal design parameters of resonating base isolators, Int. J. Mech. Sci. 224 (2022) 107284.
[12] S. Banerjee, A. Ghosh, Optimal design of nonlinear TMD with Bingham-type damping for base-excited structures, J. Struct. Integr. Maint. 5 (4) (2020) 211–222.
[13] M.C. Smith, Synthesis of mechanical networks: the inerter, IEEE Trans. Autom. Control 47 (10) (2002) 1648–1662.
[14] N.U. Islam, R. Jangid, Negative stiffness and inerter-based dampers: Novel seismic response control approach for base isolated liquid storage tanks, Struct. 60 (2024) 105860.
[15] S. Chowdhury, A. Banerjee, S. Adhikari, The optimal nonlinear inertial amplifier friction bearings for liquid storage tanks: an analytical study, Int. J. Dyn. Control. 12 (10) (2024) 3565–3576.
[16] M. Shrimali, R. Jangid, Seismic analysis of base-isolated liquid storage tanks, J. Sound Vib. 275 (1–2) (2004) 59–75.
[17] R. Jangid, Seismic analysis and performance of semi-active spring for base-isolated structures, J. Low Freq. Noise Vib. Act. Control. (2024) 14613484241290564.
[18] A. TOYOOKA, H. MOTOYAMA, O. KOUCHIYAMA, Y. IWASAKI, Development of autonomous negative stiffness damper for reducing absolute responses, Q. Rep. RTRI 56 (4) (2015) 284–290.
[19] H. Iemura, A. Igarashi, M.H. Pradono, A. Kalantari, Negative stiffness friction damping for seismically isolated structures, Struct. Control. Heal. Monit.: Off. J. Int. Assoc. Struct. Control. Monit. Eur. Assoc. Control. Struct. 13 (2–3) (2006) 775–791.
[20] H. Li, Y. Li, J. Li, Negative stiffness devices for vibration isolation applications: a review, Adv. Struct. Eng. 23 (8) (2020) 1739–1755.
[21] N. Ul Islam, R. Jangid, Seismic control and performance assessment of isolated bridges using integration of negative stiffness and inerter-based supplemental control devices, ASCE- ASME J. Risk Uncertain. Eng. Syst. A: Civ. Eng. 10 (4) (2024) 04024067.
[22] L. Ji, Y. Luo, Y. Zhang, S. Xie, M. Xu, A creative wide-frequency and large-amplitude vibration isolator design method based on magnetic negative stiffness and displacement amplification mechanism, J. Sound Vib. 572 (2024) 118185.
[23] S. Chowdhury, A. Banerjee, S. Adhikari, Enhancing seismic resilience of structures through optimally designed nonlinear negative stiffness base isolators: Exact closed-form expressions, Nonlinear Dynam. (2024) 1–24.
[24] F. Fulton, V.S. Sorokin, Analysis of the effects of nonlinear damping on a multiple-degree-of-freedom quasi-zero-stiffness vibration isolator, Mech. Res. Commun. 130 (2023) 104121.
[25] V. Matsagar, R. Jangid, Impact response of torsionally coupled base-isolated structures, J. Vib. Control 16 (11) (2010) 1623–1649.
[26] V.A. Matsagar, R. Jangid, Seismic response of base-isolated structures during impact with adjacent structures, Eng. Struct. 25 (10) (2003) 1311–1323.
[27] R. Jangid, Optimum damping in a non-linear base isolation system, J. Sound Vib. 189 (4) (1996) 477–487.
[28] S. Chowdhury, A. Banerjee, The nonlinear dynamic analysis of optimum nonlinear inertial amplifier base isolators for vibration isolation, Nonlinear Dynam. (2023) 1–38.
[29] S. Chowdhury, S. Adhikari, Nonlinear inertial amplifier liquid column dampers, Appl. Math. Model. 140 (2025) 115875.
[30] A.D. Kiureghian, A. Neuenhofer, Response spectrum method for multi-support seismic excitations, Earthq. Eng. Struct. Dyn. 21 (8) (1992) 713–740.
[31] S. Chowdhury, A. Banerjee, S. Adhikari, Optimal design of inertial amplifier base isolators for dynamic response control of multi-storey buildings, Int. J. Struct. Stab. Dyn. 23 (05) (2023) 2350047.